Hindawi Publishing Corporation
Mathematical Problems in Engineering
Volume 2014, Article ID 248676, 13 pages
http://dx.doi.org/10.1155/2014/248676

Research Article

Vehicle Chassis Integrated Control Based on Multimodel and Multilevel Hierarchical Control

Shu-en Zhao, Yuling Li, and Xian Qu

School of Mechatronics and Automobile Engineering, Chongqing JiaoTong University, Chongqing 400074, China

Correspondence should be addressed to Shu-en Zhao; zse0916@163.com

Received 19 January 2014; Accepted 17 March 2014; Published 28 April 2014

Academic Editor: Slim Choura

Aiming at the differences of vehicle chassis key subsystems influence on vehicle handling stability and effective acting regions, comprehensive considering of the nonlinear characteristic of the tires and the dynamic coupling among suspension, steering, and braking subsystems in vehicle chassis, the 14-DOF full vehicle model is built. Based on the control characteristic local optimum of each subsystem, multilevel hierarchical control theory is adopted and the vehicle stability coordinated control system including organization, coordination, and execution level is established. Using sliding mode control theory and the inverse tire model, the generalized target forces and moments from organization level are translated into the tire sideslip angle and slip ratio. And then, based on the principle of functional allocation, the control functions of each subsystem are coordinated and the function decoupling of vehicle chassis complex system is realized. The Matlab/Simulink platform is used and the full vehicle stability coordinated control system is simulated. The results show that the full vehicle coordinated control system based on multilevel hierarchical control theory can improve the vehicle stability preferably than the subsystem combined control and uncontrolled system.

1. Introduction

Vehicle chassis is a complex system which consists of steering, braking, and suspension subsystems. In order to improve the active safety, operation stability, and riding comfort of vehicle, many advanced control subsystems have appeared since the beginning of 1980s [1–5]. For the full vehicle, due to nonlinear characteristics of the tires, there is a serious dynamic coupling relationship in the vehicle longitudinal, lateral, and vertical directions. Because the active control subsystems in vehicle chassis have different objectives, this will lead to the function conflict, interference, or making the control target lack comprehensiveness.

In recent years, with the further focus on vehicle instabilities in extreme conditions and the development of the microelectronic technology and modern control theory, the vehicle chassis subsystems coordinated control have become a hot topic in the field of vehicle active safety control. Karbalaei proposed to integrate the control of active front steering (AFS) and direct yaw moment control (DYC) by the fuzzy control method; a better control effect is achieved by coordinated control wheel steering angle and yaw moment [6]. Hwang et al. studied the integrated control of AFS and ESP by supervised control strategy [7]. Ting and Lin studied integrated control of ABS and active suspension by the back stepping control [8]. Chen et al. researched on integrated control of ASS and AFS, ASS and ABS respectively by predictive control, interference suppression control and optimization control. The vehicle handling stability and riding comfort are improved significantly [9–11]. Although the integrated control of the vehicle chassis had done a lot of researches and has made full achievements, the integrated control of subsystems is achieved by the multiobjective optimization algorithm. Due to the fact that the vehicle system dynamic model is complex relatively, the integration of control strategy is very high and the controller is more difficult to design. The control system lacks flexibility and is not conducive to system expansion.

In this study, comprehensive considering of the nonlinear characteristic of tires and dynamic coupling among

suspension, steering, and braking subsystems in vehicle chassis, based on the control characteristic local optimum of each subsystem, the multilevel hierarchical control theory is adopted and the vehicle stability coordinated control system including organization, coordination, and execution level is established. According to the driver input, real-time vehicle driving condition, and ideal reference model, the upper organization level controller can get generalized target control force and moment which is the vehicle stability control needed. Based on the principle of function allocation, the control functions of subsystem are distributed by the coordination level controller and the executive level controller executes the control instructions, which are sent by coordination level. By the simulation analysis, the effectiveness of coordinated control system is verified.

2. Vehicle Nonlinear Dynamic Model

2.1. Full Vehicle Dynamic Model. Taking the steering, braking, and suspension system as the vehicle chassis key subsystems, the 14-DOF full vehicle dynamic models which contain the vehicle longitudinal, lateral, and vertical dynamics, vertical jump and the rotation of the wheels are established. According to the actual situation of vehicle system, the vehicle dynamic model assumptions and simplifications are listed as follows:

(I) assuming that the full vehicle consists of chassis, body, and tire, the vehicle quality is simplified for the sprung mass and four unsprung masses which are connected flexibly;

(II) assuming that the tires and the road are real-time contact, ignoring the impact of the vehicle air resistance, road slope, and inclination, the tire location parameters and the suspension deformation on handling stability are not considered.

Combining the force analysis of Figures 1 and 2, according to the Newton's second law, the vehicle nonlinear dynamics equations are shown as

$$\begin{aligned}
m\left(\dot{u}-v\dot{\psi}\right) &= \left(F_{x1}+F_{x2}\right)\cos\delta \\
&\quad -\left(F_{y1}+F_{y2}\right)\sin\delta + F_{x3}+F_{x4}, \\
m\left(\dot{v}+\dot{u}\dot{\psi}\right) &= \left(F_{y1}+F_{y2}\right)\cos\delta \\
&\quad -\left(F_{x1}+F_{x2}\right)\sin\delta + F_{y3}+F_{y4}, \\
I_{b,z}\ddot{\psi} &= a\left[\left(F_{y1}+F_{y2}\right)\cos\delta-\left(F_{x1}+F_{x2}\right)\sin\delta\right] \\
&\quad -b\left[\left(F_{y3}+F_{y4}\right)\right] \\
&\quad +\frac{t_f}{2}\left[\left(F_{y1}-F_{y2}\right)\sin\delta+\left(F_{x1}-F_{x2}\right)\cos\delta\right] \\
&\quad +\frac{t_r}{2}\left(F_{y3}-F_{y4}\right),
\end{aligned}$$

$$\begin{aligned}
I_{b,x}\ddot{\phi} &= h_r\left[\left(F_{y1}+F_{y2}\right)\cos\delta-\left(F_{x1}+F_{x2}\right)\sin\delta+F_{y3}+F_{y4}\right] \\
&\quad + m_b g h_0\sin\phi+\left(F_{s1}-F_{s2}\right)\frac{t_f}{2}+\left(F_{s3}-F_{s4}\right)\frac{t_r}{2}, \\
I_{b,y}\ddot{\theta} &= h_p\left[\left(F_{x1}+F_{x2}\right)\cos\delta+\left(F_{y1}+F_{y2}\right)\sin\delta+F_{x3}+F_{x4}\right] \\
&\quad +\left(F_{s3}+F_{s4}\right)b-\left(F_{s1}+F_{s2}\right)a+m_b g h_0\sin\theta, \\
m_b\cdot\ddot{x}_s &= \sum_{i=1}^{4}F_{si}, \\
m_{ui}\ddot{x}_{ti} &= k_{ti}\left(x_{ri}-x_{ti}\right)+c_{ti}\left(\dot{x}_{ri}-\dot{x}_{ti}\right)-F_{si} \quad (i=1,2,3,4), \\
I_{wi}\dot{\omega}_{wi} &= F_{xi}R_i-T_{bi} \quad (i=1,2,3,4),
\end{aligned} \tag{1}$$

where F_{xi} and F_{yi} $(i = 1,2,3,4)$ are the tire longitudinal and lateral force, respectively, which are calculated by magic formula of nonlinear tire model. F_{si} is vertical loads of the suspension. The vertical loads of the suspension are

$$\begin{aligned}
F_{s1} &= k_{s1}\left(x_{t1}-x_{s1}\right)+c_{s1}\left(\dot{x}_{t1}-\dot{x}_{s1}\right) \\
&\quad -\frac{k_{\phi f}}{2t_f}\left(\phi-\frac{\left(x_{t1}-x_{s1}\right)}{2t_f}\right)+u_1, \\
F_{s2} &= k_{s2}\left(x_{t2}-x_{s2}\right)+c_{s2}\left(\dot{x}_{t2}-\dot{x}_{s2}\right) \\
&\quad +\frac{k_{\phi f}}{2t_f}\left(\phi-\frac{\left(x_{t2}-x_{s2}\right)}{2t_f}\right)+u_2, \\
F_{s3} &= k_{s3}\left(x_{t3}-x_{s3}\right)+c_{s3}\left(\dot{x}_{t3}-\dot{x}_{s3}\right) \\
&\quad +\frac{k_{\phi r}}{2t_r}\left(\phi-\frac{\left(x_{t3}-x_{s3}\right)}{2t_r}\right)+u_3, \\
F_{s4} &= k_{s4}\left(x_{t4}-x_{s4}\right)+c_{s4}\left(\dot{x}_{t4}-\dot{x}_{s4}\right) \\
&\quad -\frac{k_{\phi r}}{2t_r}\left(\phi-\frac{\left(x_{t3}-x_{s4}\right)}{2t_r}\right)+u_4.
\end{aligned} \tag{2}$$

In the equations above, $u, v, \Psi, \theta, \Phi, \delta, \omega_{wi}$ are vehicle longitudinal velocity, lateral velocity, yaw angle, pitch angle, roll angle, steering wheel angle, and the wheel angle speed separately; m is the quality of full vehicle; m_b is sprung mass; m_{ui} is unsprung mass; $I_{b,x}, I_{b,y}, I_{b,z}$ are rotary inertia of around the x, y, z axis separately; I_{wi} is the rotary inertia of wheel; $k_{s,i}, c_{s,i}$ are suspension stiffness and damping; k_{ti} is the tire radial stiffness; $c_{t,i}$ is tire damping; x_s is the vertical displacement of vehicle body; $x_{s,i}$ is the vertical displacement of suspension; $x_{t,i}$ is the vertical displacement of tires; $k_{\phi f}, k_{\phi r}$ are the front and rear suspension roll stiffness; R_i is the wheel effective rolling radius; a and b are distances from centroid to the front and rear axle; t_f, t_r are the distances of front wheel and rear; h_0 is height of center of mass; h_r is the roll center height; h_p is pitch center height; F_{xi}, F_{yi} are tire longitudinal and lateral force separately; T_{bi} is the wheel braking torque; F_{si} is suspension vertical load; u_i is the semiactive suspension control force.

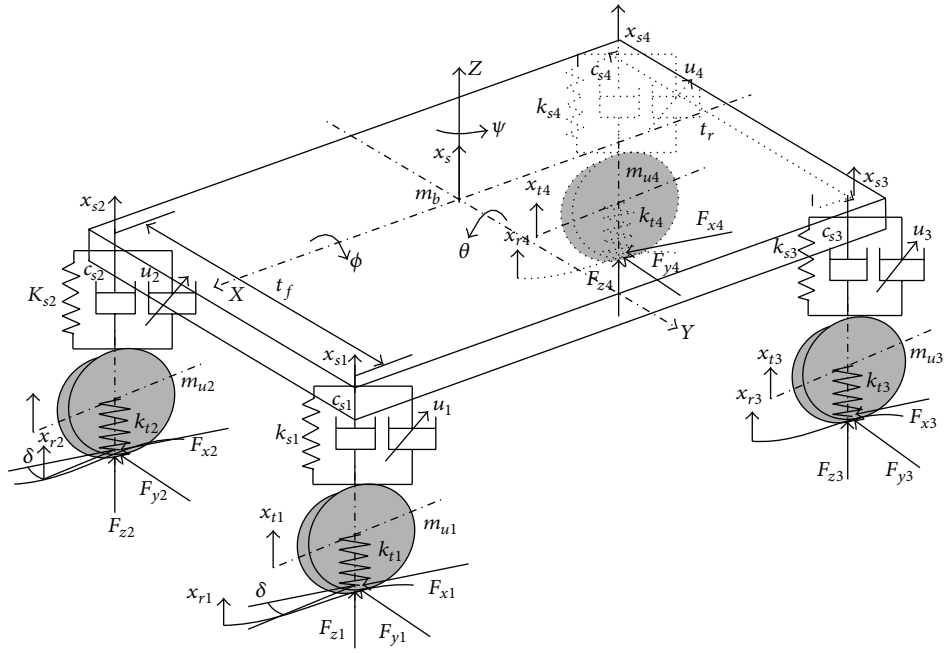

Figure 1: 14-DOF vehicle dynamic model.

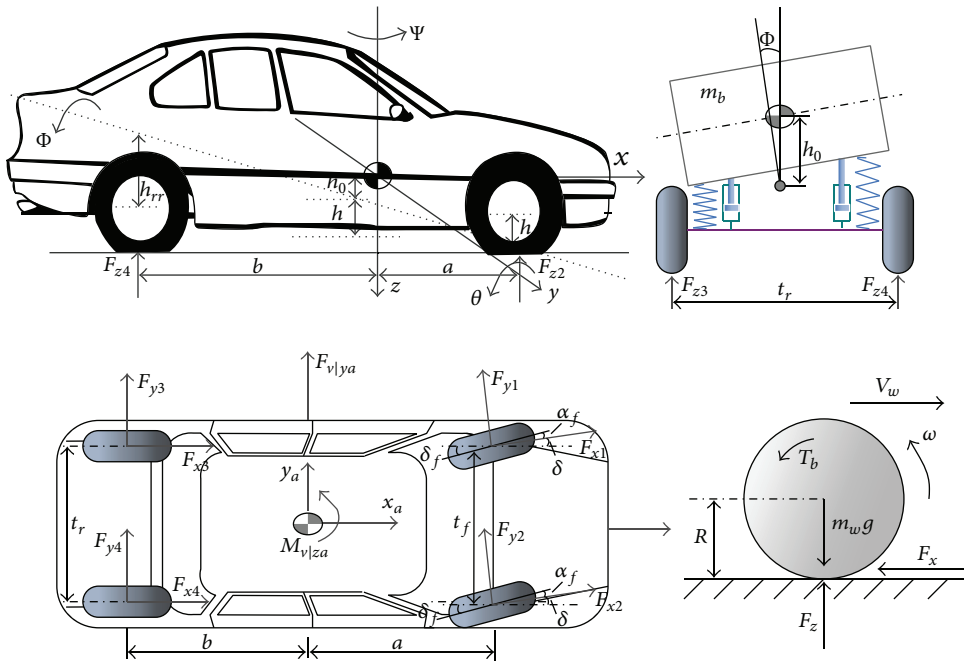

Figure 2: The vehicle force analysis.

2.2. Nonlinear Dynamic Model of the Tire. The magic formula of tire model is adopted in this study, which can express the longitudinal and the lateral force accurately by the same forms of the formula; the general expression of magic formula as follows [12]:

$$Y = D\sin\{C\arctan[B(1-E)(X+S_h) - E\arctan(B(X+S_h))]\} + Sv, \quad (3)$$

where C is the curve shape factor; D is the peak; B is the stiffness factor; E is curvature factor; S_h is horizontal shift; S_v is vertical shift. When X represents slip ratio s, Y is longitudinal force F_{x0} of the tire; when X represents the tire sideslip angle α, Y is lateral force F_{y0}. Figure 3 is original graph of the magic formula.

The longitudinal and lateral forces of the single condition are calculated by Formula (2). According to the theory of

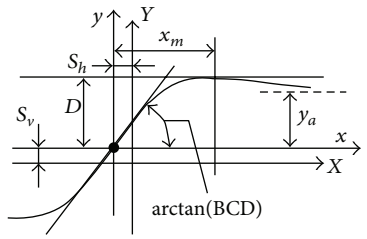

Figure 3: Original sine curve of the magic formula.

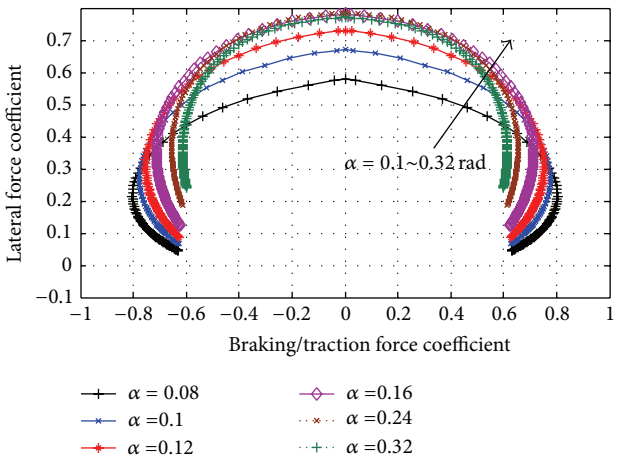

Figure 4: Tire dynamics coupling characteristics ($Fz = 4$ kN).

friction elliptic, the longitudinal force F_{xi} and lateral force F_{yi} are calculated by Formula (4) joint in the cornering and braking conditions. Figure 4 shows the tire dynamic coupling characteristics under joint working condition. Consider

$$F_{xi} = -\frac{\sigma_x}{\sqrt{\sigma_x^2 + \sigma_y^2}} F_{x0}; \qquad F_{yi} = -\frac{\sigma_y}{\sqrt{\sigma_x^2 + \sigma_y^2}} F_{y0}, \tag{4}$$

where $\sigma_x = s/(1+s)$; $\sigma_y = \tan\alpha/(1+s)$.

3. Identification of the Vehicle Stable Driving

Yaw rate and sideslip angle are important common quantities to represent the driving stability of the vehicle. Ignoring the difference of steering angle and the tire force between the left and right front wheels, the 2-DOF vehicle lateral dynamic model is simplified as follows:

$$\dot{X} = AX + BM + H\delta. \tag{5}$$

M is yaw moment of external effect; $X = [\beta \quad \dot{\psi}]^{\mathrm{T}}$,

$$A = \begin{bmatrix} \dfrac{2(k_f + k_r)}{mu} & -1 - \dfrac{2(ak_f - bk_r)}{mu^2} \\ -\dfrac{2(ak_f - bk_r)}{I_{b,z}} & -\dfrac{2(a^2k_f + b^2k_r)}{I_{b,z}u} \end{bmatrix},$$

$$B = \begin{bmatrix} 0 \\ \dfrac{1}{I_{b,z}} \end{bmatrix}, \qquad H = \begin{bmatrix} \dfrac{2k_f}{mu} & \dfrac{2ak_f}{I_{b,z}} \end{bmatrix}^{\mathrm{T}}. \tag{6}$$

According to state equation (5) of the reference model, the characteristic equation is obtained by $\det(sI - A) = 0$,

$$s^2 + K_1 s + K_0 = 0, \tag{7}$$

where

$$K_0 = \frac{2mu^2(bk_r - ak_f) + 2k_f k_r (a+b)^2}{I_{b,z} mu^2},$$
$$K_1 = \frac{2(ma^2 + I_z) + 2(mb^2 + I_{b,z})}{I_{b,z} mu}. \tag{8}$$

According to the Hurwitz stability criterion, constant and a coefficient are greater than zero to make system stabilize; that is, $K_0 > 0$, $K_1 > 0$. Apparently $K_1 > 0$; therefore, $K_0 > 0$ is only considered. Due to the fact that its denominator is nonnegative, stability condition of system is obtained by the numerator greater than 0. Consider

$$1 + \frac{u^2}{u_{\mathrm{ch}}^2} > 0, \tag{9}$$

where $u_{\mathrm{ch}}^2 = (k_f k_r (a+b))/(m(bk_r - ak_f))$ is the vehicle characteristic velocity ($u_{\mathrm{ch}}^2 \neq 0$).

When the vehicle steering radius is a certain value, the front wheel steering angle is δ_0; when the lateral acceleration is close to zero ($u_{\mathrm{ch}}^2 \to \infty$), the front wheel steering angle is δ; when it has a lateral acceleration, then the steering angle ratio of the steering wheel is

$$\frac{\delta}{\delta_0} = 1 + \frac{u^2}{u_{\mathrm{ch}}^2}. \tag{10}$$

According to Formulas (9) and (10), the state identification and stability criterion of the vehicle are achieved in different driving conditions as shown in Table 1. Where δ_L is the limit value of front wheel steering; a_x, a_{xt} are longitudinal acceleration and its expectations; $\dot{\psi}_t$ is the expectations yaw rate.

4. Vehicle Chassis Based on Multimodel and Multilevel Hierarchical Coordination Control

According to the driving condition identification and stability criterion, we take the vehicle driving stability in limiting conditions as the control target. Based on the multilevel hierarchical control theory, the multiple subsystems closed loop coordinated control system of vehicle chassis is established as shown in Figure 5.

4.1. Organizational Level Controller Based on Sliding Mode Variable Structure Control. In the limiting conditions, the

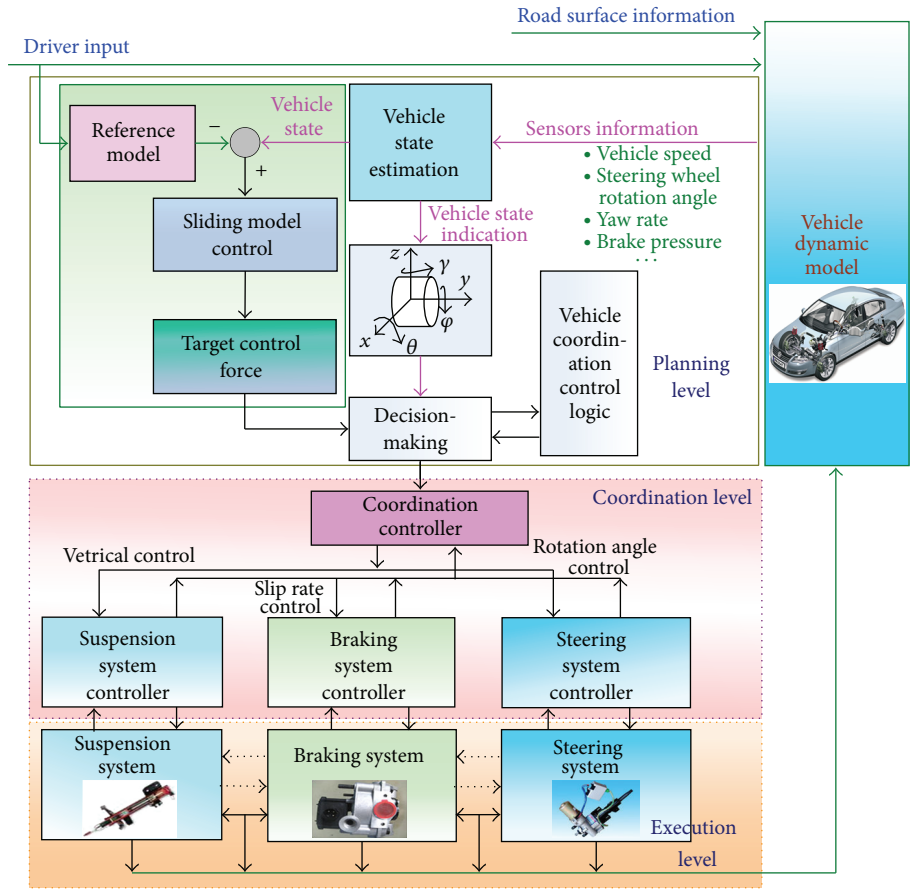

Figure 5: Vehicle chassis intelligent hierarchical control.

Table 1: Vehicle state identification and stability criterion.

Conditions	Driving state		Stability	Code
$\delta < \delta_L$ Linear mode	$\lvert\dot{\psi}\rvert \le \dot{\psi}_t; \lvert a_x\rvert < a_{xt}$	Straight	Yes	1
	$\lvert\dot{\psi}\rvert \le \dot{\psi}_t; \lvert a_x\rvert \ge a_{xt}$	braking	Yes	2
	$\lvert\dot{\psi}\rvert > \dot{\psi}_t$	Lateral	No	3
$\delta \ge \delta_L$ Steering condition	$u_{ch}^2 > 0; u_{ch}^2 \ge u^2;$ $(1 < 1 + u^2/u_{ch}^2 \le 2)$	Small understeer	Yes	4
	$u_{ch}^2 > 0; 0 < u_{ch}^2 < u^2;$ $(1 + u^2/u_{ch}^2 > 2)$	Major understeer	No	5
	$u_{ch}^2 < 0; \lvert u_{ch}^2\rvert \ge u^2$ $(0 \le 1 + u^2/u_{ch}^2 \le 1)$	Small oversteer	Yes	6
	$u_{ch}^2 < 0; \lvert u_{ch}^2\rvert < u^2$ $(1 + u^2/u_{ch}^2 < 0)$	Heated steering	No	7

main goal of vehicle driving stability control is the yaw rate and sideslip angle can well track the ideal reference value of the mode, meanwhile, keeping the wheel slip ratio near the corresponding slip ratio of the peak adhesion coefficient [13–16]. Therefore, according to the deviation between the actual value of driving condition and the ideal value of reference model, using the sliding mode variable structure control theory, the organization level controller is designed and the generalized target control force and torque are obtained so as to maintain vehicle driving stability. The generalized target control forces are converted into ideal slip angle and slip ratio of the tires by the tire inverse dynamics model. They are all the ultimate control targets of each subsystem in the multiple-model coordination control.

For the nonlinear dynamics model of full vehicle, Formula (1) is simplified appropriately and the state variables are selected. Consider

$$X = \begin{bmatrix} u & v & \dot{\psi} & \dot{x}_s & \dot{\phi} & \dot{\theta} \end{bmatrix}^{\mathrm{T}} = \begin{bmatrix} x_1 & x_2 & x_3 & x_4 & x_5 & x_6 \end{bmatrix}^{\mathrm{T}}. \tag{11}$$

Then, the related equations to characterize vehicle stability in Formula (1) can be expressed as follows:

$$\dot{X} = \begin{bmatrix} x_2 x_3 \\ -x_1 x_3 \\ 0 \\ 0 \\ 0 \\ 0 \end{bmatrix} + \begin{bmatrix} \frac{1}{m} & 0 & 0 & 0 & 0 & 0 \\ 0 & \frac{1}{m} & 0 & 0 & 0 & 0 \\ 0 & 0 & \frac{1}{m} & 0 & 0 & 0 \\ \frac{1}{m_b} & 0 & 0 & 0 & 0 & 0 \\ 0 & \frac{1}{I_{b,x}} & 0 & 0 & 0 & 0 \\ 0 & 0 & \frac{1}{I_{b,y}} & 0 & 0 & 0 \end{bmatrix} \begin{bmatrix} \sum F_{xd} \\ \sum F_{yd} \\ M_{zd} \\ \sum F_{s,i} \\ M_\phi \\ M_\theta \end{bmatrix}. \tag{12}$$

Based on the sliding variable structure control theory, the switching function is selected as follows:

$$S_i = e_i + \xi_i \varepsilon_i \quad (i = 1 \sim 6), \tag{13}$$

where $e_i = x_i - x_{id}$ is control variable error; $\varepsilon_i = \int_0^t e_i(\tau) d\tau$ is the integral of control variable error; the parameter $\xi_i > 0$. The main objective of the integral term is to limit the steady state error of the control variable.

Applying the constant speed reaching law, we get

$$\dot{S}_i = -\eta_i \operatorname{sgn}(S_i) \quad \eta_i > 0. \tag{14}$$

Then, the differential of Formula (13) is

$$\dot{S}_i = \dot{e}_i + \xi_i e_i. \tag{15}$$

Combining Formula (13) with Formula (15), we get

$$\begin{aligned}
\dot{S}_1 &= \dot{x}_1 - \dot{x}_{1d} + \xi_1 (x_1 - x_{1d}) \\
&= \left(x_2 x_3 + \frac{1}{m} \sum F_{xd} \right) - \dot{x}_{1d} + \xi_1 (x_1 - x_{1d}), \\
\dot{S}_2 &= \dot{x}_2 - \dot{x}_{2d} + \xi_2 (x_2 - x_{2d}) \\
&= \left(-x_1 x_3 + \frac{1}{m} \sum F_{yd} \right) - \dot{x}_{2d} + \xi_2 (x_2 - x_{2d}), \\
\dot{S}_3 &= \dot{x}_3 - \dot{x}_{3d} + \xi_3 (x_3 - x_{3d}) \\
&= \frac{1}{I_{b,z}} M_{zd} - \dot{x}_{3d} + \xi_3 (x_3 - x_{3d}), \\
\dot{S}_4 &= \dot{x}_4 - \dot{x}_{4d} + \xi_4 (x_4 - x_{4d}) \\
&= \frac{1}{m_b} \sum F_{sd} - \dot{x}_{4d} + \xi_4 (x_4 - x_{4d}), \\
\dot{S}_5 &= \dot{x}_5 - \dot{x}_{5d} + \xi_5 (x_5 - x_{5d}) \\
&= \frac{1}{I_{b,x}} M_\phi - \dot{x}_{5d} + \xi_5 (x_5 - x_{5d}), \\
\dot{S}_6 &= \dot{x}_6 - \dot{x}_{6d} + \xi_6 (x_6 - x_{6d}) \\
&= \frac{1}{I_{b,y}} M_\theta - \dot{x}_{6d} + \xi_6 (x_6 - x_{6d}).
\end{aligned} \tag{16}$$

Let $\dot{S}_i = 0$, in order to further eliminate the high-frequency chattering of the control input, using sgn(S) instead of saturation function. Consider

$$\operatorname{sat}\left(\frac{S_i}{\Phi_i} \right) = \begin{cases} \frac{S_i}{\Phi_i} & |S_i| < \Phi_i \\ \operatorname{sgn}(S_i) & |S_i| \geq \Phi_i, \end{cases} \tag{17}$$

where $\Phi_i > 0$ is the boundary layer thickness. Then, the generalized target control force and torque to achieve vehicle stability control are shown in the following formula:

$$F_{ud} = \begin{bmatrix} \sum F_{xd} \\ \sum F_{yd} \\ M_{zd} \\ \sum F_{sd} \\ M_\phi \\ M_\theta \end{bmatrix} = \begin{bmatrix} m [\dot{u}_d - v\dot{\psi} - \xi_1 e_1 - \eta_1 \operatorname{sat}(S_1)] \\ m [\dot{v}_d - u\dot{\psi} - \xi_2 e_2 - \eta_2 \operatorname{sat}(S_2)] \\ I_{b,z} [\ddot{\psi}_d - \xi_3 e_3 - \eta_3 \operatorname{sat}(S_3)] \\ m_b [\ddot{x}_{sd} - \xi_4 e_4 - \eta_4 \operatorname{sat}(S_4)] \\ I_{b,x} [\ddot{\phi}_d - \xi_5 e_5 - \eta_5 \operatorname{sat}(S_5)] \\ I_{b,y} [\ddot{\theta}_d - \xi_6 e_6 - \eta_6 \operatorname{sat}(S_6)] \end{bmatrix}. \tag{18}$$

Because the wheel longitudinal and lateral force are functions about slip ratio and slip angle of tires, according to the tire inverse model [17, 18], the longitudinal target control force F_{xd} and the lateral target control force F_{yd} are transformed into the tire longitudinal target slip ratio s_{di} and sideslip angle α_{di}.

Assuming the generalized target control forces F_{xd}, F_{yd}, M_{zd} are shown in the following equation:

$$F_{ud} = \begin{bmatrix} F_{xd} & F_{yd} & M_{zd} \end{bmatrix}^{\mathrm{T}} = B \cdot U, \tag{19}$$

where U is tire force vector; B is matrix of the tire force. Consider

$$U = \begin{bmatrix} F_{x1} & F_{y1} & F_{x2} & F_{y2} & F_{x3} & F_{y3} & F_{x4} & F_{y4} \end{bmatrix}^{\mathrm{T}}. \tag{20}$$

Suppose U_c is the middle control input. It includes the sideslip angle and slip ratio of four tires. Consider

$$U_c = \begin{bmatrix} s_{fl} & s_{fr} & s_{rl} & s_{rr} & \alpha_{fl} & \alpha_{fr} & \alpha_{rl} & \alpha_{rr} \end{bmatrix}^{\mathrm{T}}, \tag{21}$$

where s_{fl}, s_{fr}, s_{rl}, s_{rr} are longitudinal slip ratio and $\alpha_{fl}, \alpha_{fr}, \alpha_{rl}, \alpha_{rr}$ are sideslip angle of four tires.

The control inputs of tires including the front wheel steering angle δ and the control torque T_b are obtained by controlling the steering angle of the active steering system and longitudinal slip ratio of the braking system.

With Formula (19), the matrix of tire force is as follows:

$$B = \begin{bmatrix} B_1 & B_2 & B_3 \end{bmatrix}^{\mathrm{T}} = \begin{bmatrix} \frac{\partial F_{xd}}{\partial U_c} & \frac{\partial F_{yd}}{\partial U_c} & \frac{\partial M_{zd}}{\partial U_c} \end{bmatrix}^{\mathrm{T}}. \tag{22}$$

Because the matrix B of tire force is not a square matrix, the assigned tire forces are not obtained directly. So, using the unconstrained optimization, the generalized target control forces for tires can be distributed.

From the nonlinear dynamic model of tires, the ideal control forces or torques are got from organizational level in the hierarchical control of vehicle chassis [4]. It is a nonlinear function about the control system configuration parameters and control input elements as follows:

$$F_{ud} = g(\phi, U), \tag{23}$$

where $\phi = [F_{zi} \ \ \mu \ \ \delta]^{\mathrm{T}}$; F_{zi} are vertical loads of the tire; μ is road friction coefficient; δ is steering angle.

Formula (23) is linearized about working identification point as follows:

$$g(\phi, U_k) \approx g(\phi, U_{k-1}) + \frac{\partial g}{\partial U}(\phi, U_{k-1}) \cdot (U_k - U_{k-1}),$$

$$g(\phi, U_k) - g(\phi, U_{k-1}) + \frac{\partial g}{\partial U}(\phi, U_{k-1}) U_{k-1} \tag{24}$$

$$\approx \frac{\partial g}{\partial U}(\phi, U_{k-1}) U_k,$$

$$\overline{F}_{ud} = B(\phi, U_{k-1}) \cdot U_k, \tag{25}$$

$$\overline{F}_{ud} = F_{ud} - g(\phi, U_{k-1}) + \frac{\partial g}{\partial U}(\phi, U_{k-1}) U_{k-1}. \tag{26}$$

In Formula (25), $B(\phi, U_{k-1}) = (\partial g/\partial U)(\phi, U_{k-1})$ is the Jacobian about the point(ϕ, U_{k-1}); that is, it is a working matrix of operation system, which is obtained by the tire model of magic formula.

Let the incremental ΔU_c of middle control input U_c be

$$\Delta U_c = [\Delta s_{fl} \ \ \Delta s_{fr} \ \ \Delta s_{rl} \ \ \Delta s_{rr} \ \ \Delta\alpha_{fl} \ \ \Delta\alpha_{fr} \ \ \Delta\alpha_{rl} \ \ \Delta\alpha_{rr}]^{\mathrm{T}}. \tag{27}$$

At the $(k+1)$th sampling time, the vehicle control force F_u is generated by the four wheels, and it can be approximated as follows:

$$F_u(k+1) \approx F_u(k) + B \cdot \Delta U_c. \tag{28}$$

According to the control objectives and constraints of the tire force distribution, the objective function is proposed as follows:

$$J_1 = E^{\mathrm{T}} W_E E + \Delta U_c^{\mathrm{T}} W_{\Delta U_c} \Delta U_c + U_c^{\mathrm{T}} W_{U_c} U_c, \tag{29}$$

where $W_E, W_{\Delta U_c}$, and W_{U_c} are weight matrices which represent force tracking error, control input increment, and control input amplitude, respectively.

The difference between vehicle target control force and current control forces is

$$\widetilde{E} = F_{ud} - F_u(k). \tag{30}$$

Then,

$$E = \widetilde{E} - B \cdot \Delta U_c. \tag{31}$$

Plug Formulas (28) and (31) into Formula (29), with the minimum objective function; let $\partial J_1/\partial \Delta U_c = 0$; then, the optimal control variable increments of tire can be achieved as follows:

$$\Delta U_c^d = \left(W_{U_c} + W_{\Delta U_c} + B^{\mathrm{T}} W_E B\right)^{-1} \left[B^{\mathrm{T}} W_E \widetilde{E} - W_{U_c} U_c(k)\right]. \tag{32}$$

Then, the target control input for tire actuator is assigned as follows:

$$U_c^d = [s_{di} \ \ \alpha_{di}]^{\mathrm{T}} = U_c(k) + \Delta U_c^d. \tag{33}$$

Translating the longitudinal target control force F_{xd} into the tire slip ratio, it can be realized by ABS and SAS active control. At the same time, changing the lateral control target force into the tire sideslip angle, it can be realized by AFS system. Vehicle yaw generalized target torque Mz can be realized by coordinated control of steering and braking systems. The vertical, roll, and pitch generalized objective control forces and torques $\sum F_{sd}$, M_ϕ, and M_θ are translated into equivalent control force of four semiactive suspensions, and they participate in coordinated control among the other subsystems and improve the vehicle driving stability and safety.

4.2. Coordination Level Controller Based on Multimodel Hierarchical Control. According to the vehicle driving state identification and the stability judgment rules as shown in Table 1, the vehicle of each subsystem is coordinated control and the vehicle real states are identified and decided. Then, the main control objectives are confined to the corresponding working conditions. Meanwhile, they are an important basis for subsystem task assignment. Consider the following.

(I) When the vehicle is in stable condition, according to the requirements of the actual driving status, the vehicle active subsystems of AFS, ABS, and SAS are controlled with each optimal control.

(II) When the vehicle is in an unsteady operation such as the separation coefficient road, high-speed steering, and braking, because of the AFS control performance and structure limitation, the tracking control of larger yaw moment cannot achieve well. At this moment, ABS can put the different braking torque to the wheel to obtain larger yaw moment. Meanwhile, SAS takes part in the vehicle stability control to control the vehicle vertical load. According to the control strategy of coordination level controller and the generalized control target of organizational level controller, the control goals are assigned to ABS, AFS, and SAS.

(III) When the vehicle chassis subsystems are coordinated control, the additional yaw moment generated by ABS through wheels assist brake is

$$M_{za} = q_a M_{zd}. \tag{34}$$

Then, the goal yaw moment achieved by AFS is

$$M_{ze} = (1 - q_a) M_{zd}, \tag{35}$$

where q_a is a weight coefficient. When ABS controls independently, $q_a = 1$; when AFS works independently, $q_a = 0$; when the vehicle chassis subsystems are coordinated control, in order to prevent generating great shock in the switch process, q_a is calculated by continuous function Sigmoid. The expression of Sigmoid function is shown as follows:

$$y = \frac{1}{1 + e^{-a(x-c)}}, \tag{36}$$

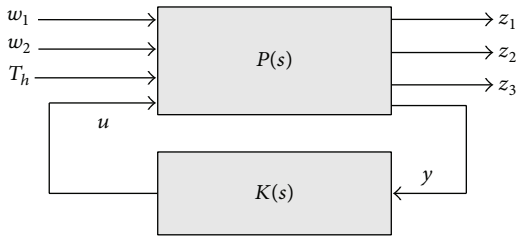

Figure 6: The standard structure of AFS H_∞ robust control.

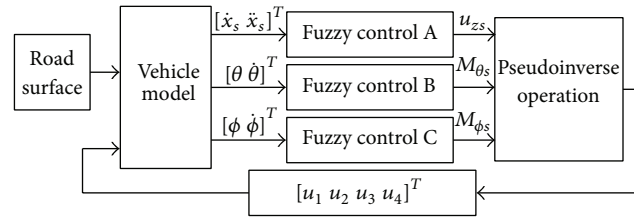

Figure 7: Suspension system controller frame.

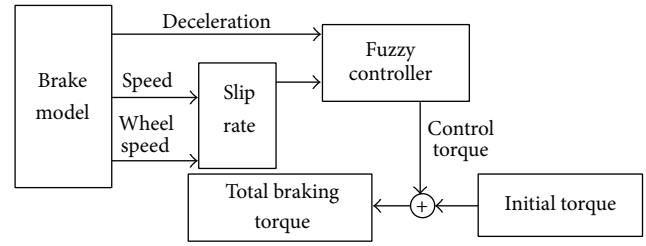

Figure 8: Fuzzy controller structure of ABS.

where a, c are constant greater than zero, and they represent the control shape and position of function, respectively.

According to the lateral acceleration, the additional control force of the SAS system is given as follows:

$$u_s = k\left|a_y - \operatorname{sgn}\left(a_y\right) a_{yr}\right|, \tag{37}$$

where the parameter k is adjusted with the lateral acceleration to achieve coordination control with other subsystems.

4.3. Execution Level Controller Based on Multimodel Hierarchical Control

4.3.1. AFS Controller Based on H_∞ Robust Control. According to the performance requirements of AFS steering system and the vehicle steering stability control target, the H_∞ robust control theory is used to study its control characteristics [7, 19]. The standardized form of AFS steering system with H_∞ control is shown in Figure 6.

In Figure 6, $W = \left[w_1\ w_2\ T_h\right]^{\mathrm{T}}$ are external input variables; where w_1 is road noise; w_2 is measuring noise; T_h is steering wheel control torque; $Z = \left[E_a\ E_f\ E_r\right]^{\mathrm{T}}$ are output variables of the system performance evaluation; $y = \left[\dot{\psi}\ \beta\ T_a\ T_s\right]^{\mathrm{T}}$ is the measured variable; the control input signal $u = [T_m]$ is electromagnetic torque. $P(s)$ is transfer function from the input signal u, w to the output signal z, y; $k(s)$ is the controller.

In order to ensure drivers road-feel and the sensitivity of EPS, let the weighting function $w_1(s)$, $w_2(s)$ be as follows:

$$\begin{aligned} w_1(s) &= \frac{30.5}{0.000196s^3 + 0.013333s^2 + 0.2s + 1}, \\ w_2(s) &= \frac{0.015s + 0.00015}{0.001s + 1.056}. \end{aligned} \tag{38}$$

In order to make H_∞ controller of AFS system meet the AFS assisted steering requirements and the vehicle handling stability control objectives, the choice principles about system evaluation output variables E_a, E_f and E_r are complied with the following rules:

(I) make $\|E_a\|_\infty = \|T_a - T_{ad}\|_\infty$ minimal, to ensure the offset between the actual motor assist torque T_a generated by motor and the ideal motor assist torque T_{ad} is minimum;

(II) make $\|E_f\|_\infty = \|T_s - T_{sd}\|_\infty$ minimal to reduce the interference of the road surface and ensure a good steering feel;

(III) make $\|E_r\|_\infty = \|\dot{\psi} - \dot{\psi}_d\|_\infty$ minimal to access the vehicles real yaw rate to the ideal yaw rate and ensure a good handling stability.

4.3.2. SAS Controller Based on Fuzzy Control. Taking the body vertical acceleration and velocity, pitch angle acceleration and velocity, and roll angle acceleration and velocity as the controller inputs, where the vertical, pitch, and roll equivalent control force and moment are the controller outputs, three independent fuzzy controllers are designed. And then, by pseudoinverse calculation, the active control forces of four suspensions are achieved. By this way, the vehicle riding comfort and handling stability are improved. The structure of semiactive suspension fuzzy controller is shown in Figure 7.

Combine the vehicle system dynamics equations in Formula (1), $t_f/2 = t_r/2 = d$. Using the pseudoinverse operation, the goal control force of four semiactive suspensions is given as follows:

$$\begin{bmatrix} u_1 \\ u_2 \\ u_3 \\ u_4 \end{bmatrix} = \begin{bmatrix} \frac{b}{2(a+b)} & \frac{1}{2d\cos\phi} & \frac{1}{2(a+b)\cos\theta} \\ \frac{b}{2(a+b)} & -\frac{1}{2d\cos\phi} & \frac{1}{2(a+b)\cos\theta} \\ \frac{a}{2(a+b)} & \frac{1}{2d\cos\phi} & -\frac{1}{2(a+b)\cos\theta} \\ \frac{a}{2(a+b)} & -\frac{1}{2d\cos\phi} & -\frac{1}{2(a+b)\cos\theta} \end{bmatrix} \begin{bmatrix} u_{zs} \\ M_{\phi s} \\ M_{\theta s} \end{bmatrix}. \tag{39}$$

4.3.3. ABS Controller Based on Fuzzy Control. Based on the fuzzy control theory, taking the slip ratio λ and vehicle deceleration a_x as the controller inputs, adjusting torque T_c as the output, the ABS fuzzy controller is designed. The structure of ABS controller is shown in Figure 8.

Table 2: The main parameters of the constructed vehicle.

Parameter	Value
m [kg]	1527
m_{u1}, m_{u2} [kg]	49.05
m_{u3}, m_{u4} [kg]	39.85
h_0 [m]	0.5
h_p [m]	0.4
h_r [m]	0.25
$I_{b,x}$ [kg·m^2]	744
$I_{b,y}$ [kg·m^2]	2160
$I_{b,z}$ [kg·m^2]	3048
I_{wi} [kg·m^2]	0.99
R [m]	0.313
a [m]	1.035
b [m]	1.655
t_f [m]	1.535
t_r [m]	1.535
k_{s1}, k_{s2} [N/m]	29509
k_{s3}, k_{s4} [N/m]	27126
c_{s1}, c_{s2} [N·s/rad]	1767
c_{s3}, c_{s4} [N·s/rad]	1542
k_{ti} [N/m]	181000
$k_{\phi f}$ [N·m/rad]	47298
$k_{\phi r}$ [N·m/rad]	37311

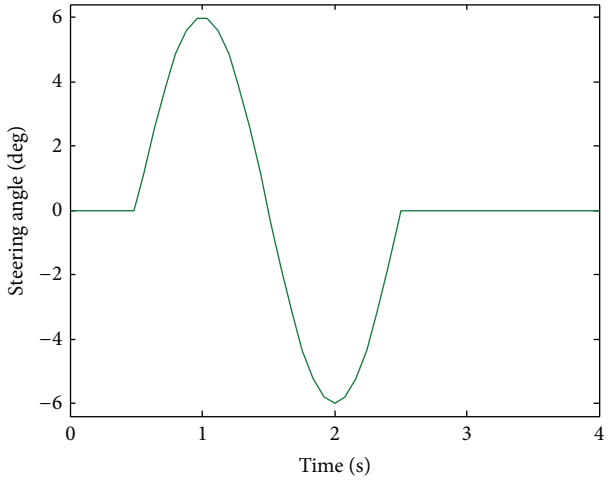

Figure 9: Steering angle of single lane change.

5. Simulation and Analysis

Applying the simulation software of Matlab/Simulink, taking a vehicle as an example, the control strategy of vehicle chassis integrated control based on multimodel and multilevel hierarchical control is simulated. The parameters of vehicle are shown in Table 2.

5.1. Simulation and Analysis in Single Line Condition. Assuming the vehicle velocity is 30 m/s, driving at B class road surface, the front wheel steering input is a sine signal, in which frequency is 0.5 Hz and amplitude is 6°, as shown in Figure 9.

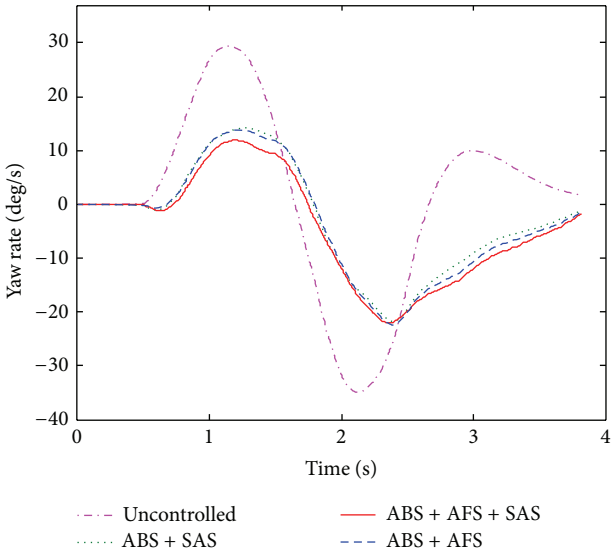

Figure 10: Vehicle body yaw rate.

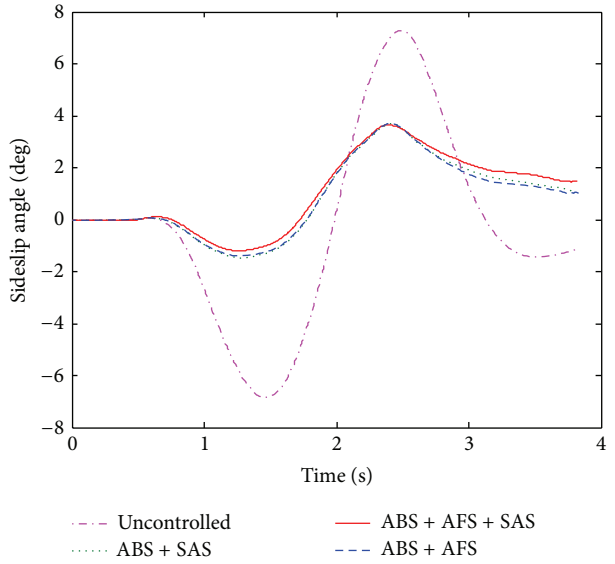

Figure 11: Vehicle body sideslip angle.

Figures 10, 11, 12, and 13 are showing that the response curves of the vehicle when yaw-rate, the sideslip angle, roll angle, and pitch angle, respectively. As shown in these figures, using different coordination control strategy between ABS, AFS, and SAS can improve the vehicle lateral stability. For ABS and SAS combined control, the vehicle stability control effect is poor relatively. This is because the main target of SAS vertical auxiliary role is to enhance the braking safety in this control strategy, that is, the vertical load and braking torque with the same phase changing. In addition, the simulation results also show that AFS can improve the vehicle handling stability effectively when the yaw rate is large, also the yaw

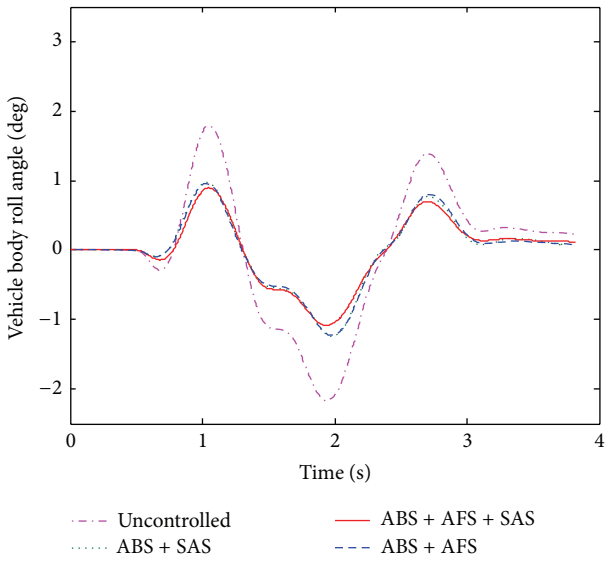

Figure 12: Vehicle body roll angle.

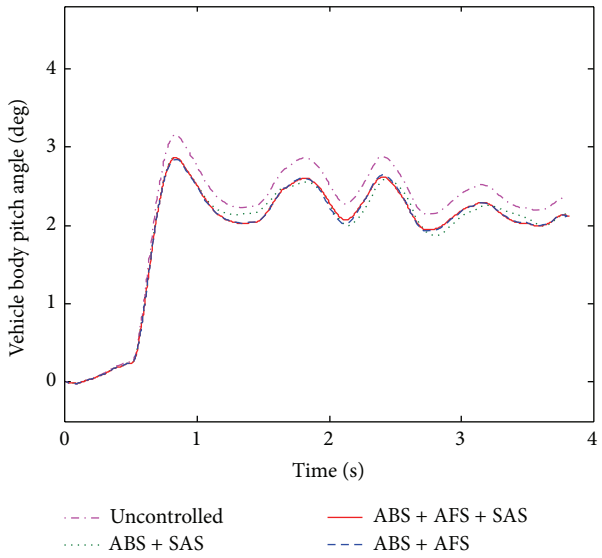

Figure 13: Vehicle body pitch angle.

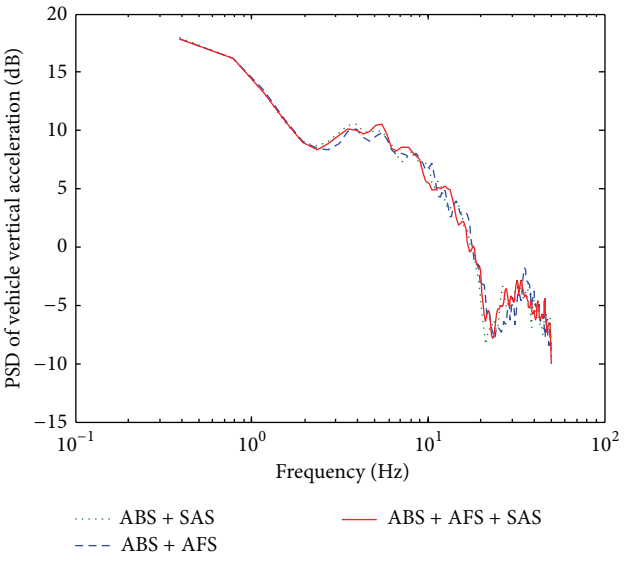

Figure 14: PSD of vehicle vertical acceleration.

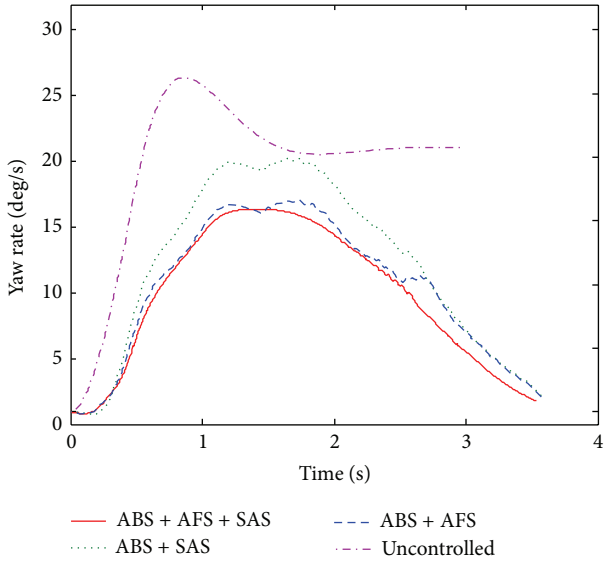

Figure 15: Vehicle body yaw rate.

rate amplitude jitter is minimal when ABS, AFS, and SAS are comprehensive coordination control. The change trend of vehicle side-slip angle is the same as the yaw rate. Figure 14 shows that the vehicle body vertical acceleration amplitude is reduced with coordinated control method. It indicates that ABS, AFS, and SAS subsystem integrated control based on multimodel and multilevel hierarchical control not only improves the vehicle handling stability, but also it improves the riding comfort.

5.2. Simulation and Analysis with Step Steering Angle. Assuming the vehicle velocity is 30 m/s, driving at B class road surface, the front wheel steering input is a step signal, in which amplitude is 6°, and after 0.3 s, the vehicle starts braking. When the vehicle is in emergency turning and braking condition, the multisubsystem coordinated control strategy is simulated and the results are shown in Figures 15, 16, 17, 18, 19, 20, 21, and 22.

Figures 15 to 18 are showing that the response curves of the vehicle when yaw-rate, the sideslip angle, roll angle and pitch angle, respectively. As shown in these figures, the vehicle handling stability with the vehicle chassis subsystem of ABS and SAS joint control is poor relatively. The reason for this is the vehicle has worked in the unstable state in the condition of steering and braking. The lateral auxiliary control function of ABS is limited. While, the main target of SAS is to improve the vehicle braking safety and comfort. In addition, the simulation results indicate that AFS can improve the vehicle handing stability and reduce the vehicle roll and

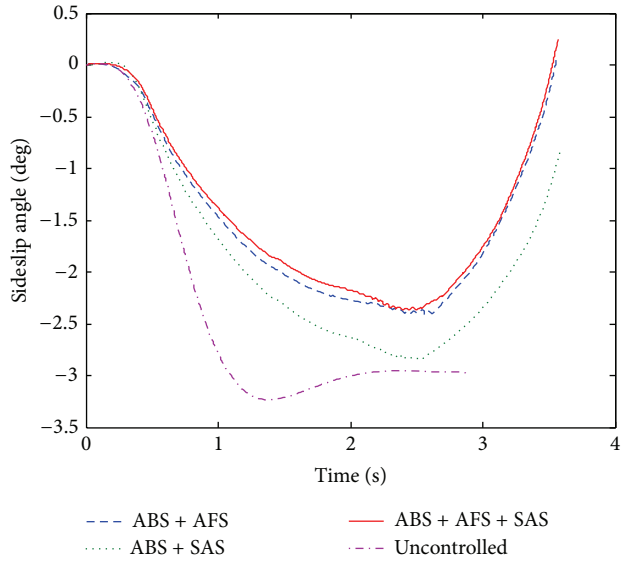

Figure 16: Vehicle body sideslip angle.

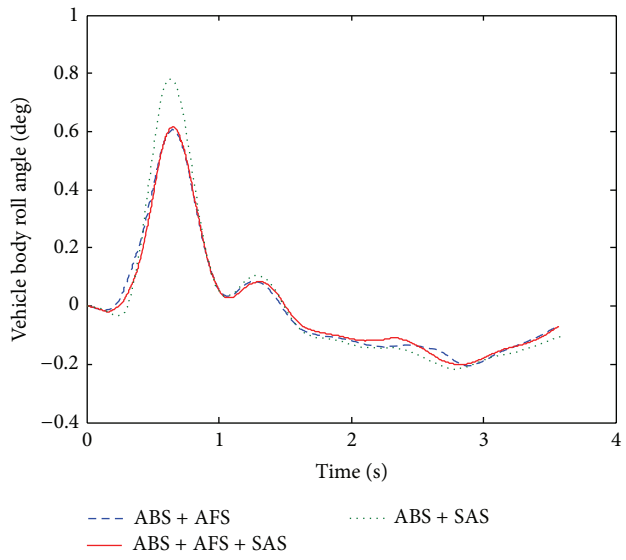

Figure 17: Vehicle body roll angle.

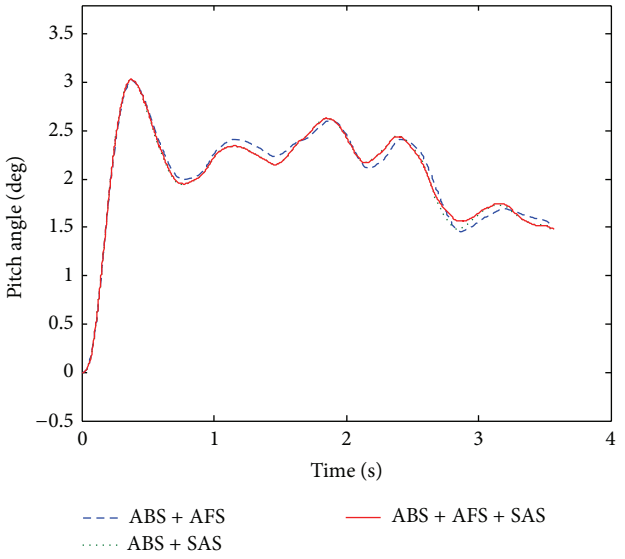

Figure 18: Vehicle body pitch angle.

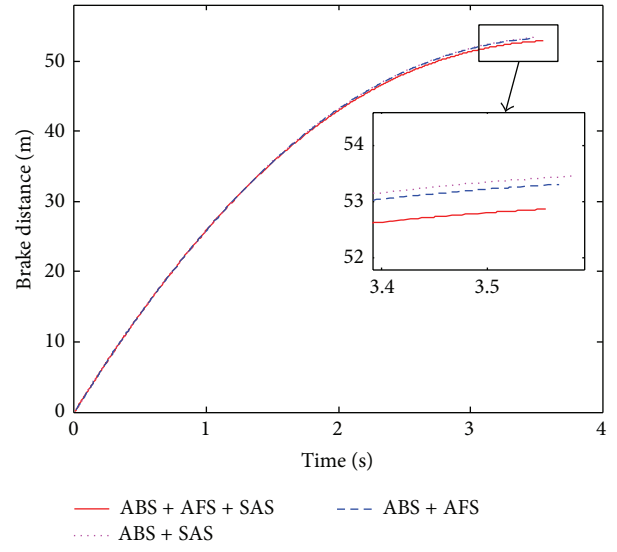

Figure 19: Braking distance.

pitch angle obviously. The yaw rate amplitude jitter is minimal with multisubsystem coordinated control and enables the vehicle to reach steady state quickly.

Figures 19 to 22 represent the response curves of vehicle braking distance and the longitudinal slip ratio of front and rear wheels, respectively. The figures show that the braking distance is reduced, the braking time is shortened, and the slip ratio keeps near the target value 0.2 with the coordinated control strategy of ABS, AFS, and SAS. This is due to the wheel vertical load consistent with the braking torque with SAS control. Therefore, it improves the braking ability of the full vehicle. Figure 22 shows that the vertical acceleration of vehicle body is reduced. It indicates that the vehicle chassis integrated control based on multimodel and multilevel hierarchical control can improve the vehicle handling stability and the riding comfort effectively.

6. Conclusions

(I) Based on the multilevel hierarchical control theory and function assignment principle, the generalized target control force or torque for controlling the vehicle stability is transformed into the control target of vehicle chassis key subsystem with the tires inverse dynamics model and pseudoinverse calculation. So, the function decoupling of the vehicle nonlinear

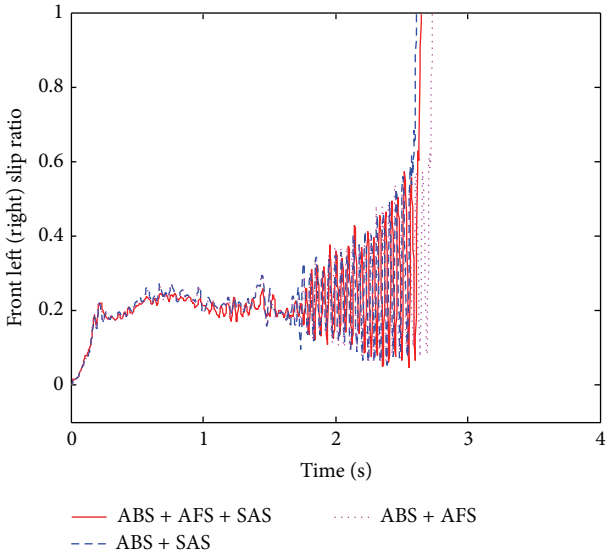

Figure 20: Front wheel slip ratio.

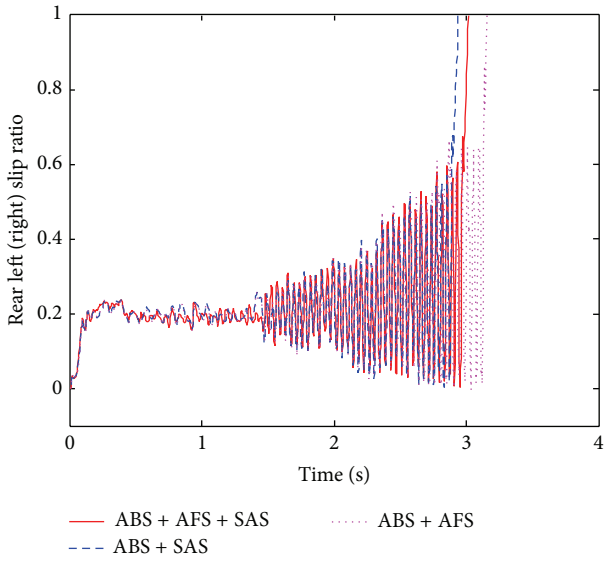

Figure 21: Rear wheel slip ratio.

dynamics coupling and the vehicle chassis multimodel coordinated control in the extreme conditions are realized.

(II) The vehicle chassis multimodel and multilevel hierarchical control strategy can suppress the interference among multisubsystems to some extent and improve the vehicle handling stability, active safety, and riding comfort effectively.

Conflict of Interests

The authors declare that there is no conflict of interests regarding the publication of this paper.

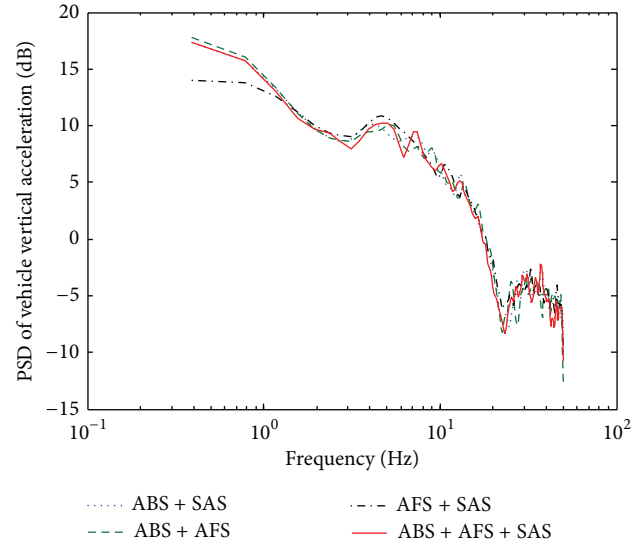

Figure 22: PSD of vehicle vertical acceleration.

Acknowledgments

Authors would like to thank anonymous reviewers and the editor for their valuable comments and the National Natural Science Foundation of China (no. 51278514) and the Special Fund of Chongqing Education Commission (KJ120415) and the Special Fund of Shaanxi Education Department (12JK0693) for their sponsorship.

References

[1] S. J. Semmler and P. E. Rieth, "Global chassis control the networked chassis," SAE Paper 2006-01-1954, 2006.

[2] Y. Shibahata, "Progress and future direction of Chassis control technology," *Annual Reviews in Control*, vol. 29, no. 1, pp. 151–158, 2005.

[3] H. Chen, X. Gong, and Y.-F. Hu, "Automotive control: the state of the art and perspective," *Acta Automatica Sinica*, vol. 39, no. 1, pp. 1–25, 2013.

[4] M. Nagai, "Perspectives of research for enhancing active safety based on advanced control technology," *Journal Automotive Safety and Energy*, vol. 1, no. 1, pp. 14–22, 2010.

[5] P. Kvasnicka and P. Dick, "Integrated development of vehicle dynamics demonstrated on the new BMW 3 series," in *Proceedings of the FISITA World Automotive Congress*, pp. 379–389, 2012.

[6] R. Karbalaei, A. Ghaffari, and R. Kazemi, "A new intelligent strategy to integrated control of AFS/DYC based on fuzzy logic," *International Journal of Mathematical, Physical and Engineering Sciences*, vol. 1, no. 1, pp. 47–52, 2008.

[7] T. H. Hwang, K. Park, and S. J. Heo, "Design of integrated chassis control logics for AFS and ESP," *International Journal of Automotive Technology*, vol. 9, no. 1, pp. 17–27, 2008.

[8] W. Ting and J. Lin, "Nonlinear control design of anti-lock braking systems with assistance of active suspension," *IET Control Theory & Applications*, vol. 1, no. 1, pp. 611–616, 2007.

[9] X. Liu and W. Chen, "Coordinated control between direct yaw moment control and anti-block braking system used for ESP," *Journal of Agricultural Machinery*, vol. 40, no. 4, pp. 1–6, 2009.

[10] W. Chen and H. Zhou, "Simulation research on layered coordinated control of automotive ESP and ASS," *Chinese Journal of Mechanical Engineering*, vol. 45, no. 8, pp. 190–196, 2009.

[11] H. Wang, W. Chen, and Y. Liuqing, "Coordinated control of vehicle chassis system based on game theory and function distribution," *Chinese Journal of Mechanical Engineering*, vol. 48, no. 22, pp. 105–112, 2012.

[12] M. S. Burhaumudin and P. M. Samin, "Integration of magic formula tire model with vehicle handling model," *International Journal of Research in Engineering and Technology*, vol. 1, no. 3, pp. 139–145, 2012.

[13] A. Trächtler, "Integrated vehicle dynamics control using active brake, steering and suspension systems," *International Journal of Vehicle Design*, vol. 36, no. 1, pp. 1–12, 2004.

[14] P. Koehn and M. Eckrich, "Integrated chassis management: introduction into BMW's approach to ICM," SAE Paper 2006-01-1219, 2006.

[15] J. Diebold, "Active safety systems-the home for global chassis control," SAE Paper 2006-21-0079, 2006.

[16] A. Jarašuniene and G. Jakubauskas, "Improvement of road safety using passive and active intelligent vehicle safety systems," *Transport*, vol. 22, no. 4, pp. 284–289, 2007.

[17] Y. Liu, M. Fang, and H. Wang, "Forces calculation and distribution in vehicle stability control," *Control Theory and Applications*, vol. 30, no. 9, pp. 1122–1130, 2013.

[18] X. Shen and F. Yu, "Investigation on integrated vehicle chassis control based on vertical and lateral tyre behaviour correlativity," *Vehicle System Dynamics*, vol. 44, no. 1, pp. 506–519, 2006.

[19] C. March and T. Shim, "Integrated control of suspension and front steering to enhance vehicle handling," *Journal of Automobile Engineering*, vol. 221, no. 4, pp. 377–391, 2007.